Nearly-Automated Quantification of Mitral Annulus and Leaflet Morphology from Transesophageal Real-Time 3D Echocardiography

Miguel Sotaquira[1], Laura Fusini[2], Roberto M Lang[3], Enrico G Caiani[1]

[1]Politecnico di Milano, Milan, Italy
[2]Centro Cardiologico Monzino IRCCS, Milan, Italy
[3]University of Chicago Hospitals, Chicago, IL, USA

Abstract

The ability to extract and quantify three-dimensional (3D) morphological parameters of the mitral valve (MV) apparatus from transesophageal 3D echocardiographic (T3DE) imaging constitutes a valuable tool in diagnosis, treatment and follow-up of patients with MV disease. Mitral annulus (MA) and leaflets (ML) quantification is still challenging, and commonly based on intensive user interaction that limits its applicability. We proposed a fast and accurate model-free, nearly-automated method for segmenting and extracting MA and ML morphological parameters, requiring a set of only 8 user-defined points. The algorithm accuracy was tested on 12 patients compared to "gold standard" manual analysis, resulting in narrow limits of agreement, and good inter- and intra-observer variability, except for MA height computation. The proposed technique appears promising for clinical application.

1. Introduction

Mitral annulus (MA) and leaflets (ML) morphological quantification has proven being a valuable input in diagnosis, treatment and follow-up of patients with mitral valve (MV) disease. In recent years, transesophageal (TEE) real-time 3D echocardiography (T3DE) has made possible the assessment of the 3D intrinsic MV structure, given the MA and ML intrinsic 3D morphology, thus leading T3DE as the clinical standard for MV evaluation during intraoperatory assessment[1].

However, quantification of MA and ML morphological parameters from T3DE volumes remains a challenging task, and commonly used strategies rely on manual, user intensive segmentation procedures. More recently, semi-automated approaches have been proposed for segmenting both the MA[2] and the ML[3, 4], even if in these cases leaflets segmentation was achieved only in open valve configurations [3] or by incorporating a collision model to estimate the location of leaflets tips during closure [4].

We hypothesized that the T3DE dataset contains intrinsic information that could further be exploited to minimize the required user interaction for MV analysis, and allowing quantification of additional parameters of potential clinical interest. Accordingly, our aims were: 1) to develop a new nearly-automated method for MA segmentation at closed valve from the T3DE data, followed by a fully automated ML segmentation; 2) to extract morphological parameters from segmented MA and ML; 3) to test the accuracy of this analysis compared to a manual "gold standard", and evaluate its reproducibility.

2. Methods

2.1. Population and imaging protocol

Data from 12 patients (mean age 50 ± 10) enrolled at the University of Chicago Hospitals (Chicago, IL), undergoing clinically indicated TEE imaging for assessment of a stroke cardioembolic source were considered. The protocol was approved by the local Institutional Review Board, and informed consent was obtained from all participants. T3DE studies were performed using the iE33 system (Philips Medical Systems, Andover, MA) equipped with fully sampled matrix-array TEE transducer (X7-2t): the probe was positioned at the midesophageal level with a 120° tilt and images acquired using the wide-angled acquisition mode, in which ECG-triggered wedge-shaped subvolumes were obtained over four consecutive cardiac cycles. Each acquired volume included the MV, the aortic valve and the proximal ascending aorta.

2.2. Mitral annulus initialization

The end-systolic (ES) frame was selected for the analysis: a) from the T3DE volume the user first selects a 2D cut-plane corresponding to the 3-chamber view, to identify the anterior (*A*) and posterior (*P*) annular points (Figure 1, top left), from which the annulus center is computed as the *AP* segment middle point; b) an additional 2D cut-

plane, passing through the annulus center and orthogonal to the first plane, is shown for selection of the Antero-lateral (*Al*) and Postero-medial (*Pm*) annular points (Figure 1, top right); c) a set of 4 points symmetrically positioned around *A* are selected on evenly-rotated (30° apart) 2D cut-planes. Figure 1 (bottom) depicts the location of the 8 user-defined points.

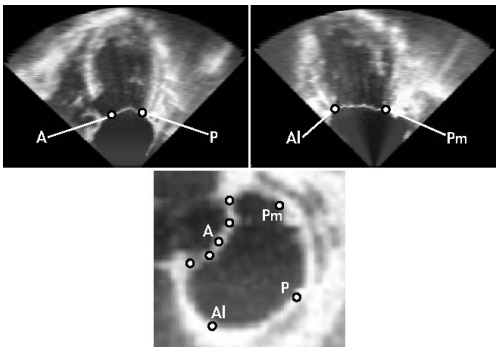

Figure 1. Manual initialization of the MA segmentation algorithm (see text for details).

The annulus center *c* is then used for generating a set of 36 evenly rotated (5° apart) 2D cut-planes, that constitute the input for the next steps of the analysis.

2.3. Mitral annulus segmentation

As the location of the MA is known for the 8 user-defined points, the challenge is to locate the remaining 64 points on the corresponding rotational cut-planes. To do so, each user-defined point is tracked in space using a modified block-matching technique along with a graph search algorithm[5]. This is performed by iterating between consecutive pairs of initialized points, and terminating when all the 64 MA points have been computed.

To do so, first a region-of-interest (ROI) image is defined around each initialized point, with a region-of-search (ROS) obtained in the contiguous cut-plane. Then, two feature images are computed:

1. *Weighted-normalized cross-correlation (WNCC)*, that measures the similarity of gray patterns between ROI and ROS, and it is expected to reach its maximum near the annular locations.

2. *Enhanced junction detector (EJD)* that represents the probability image, using ROS as input, where regions most likely containing a junction point (i.e., a MA point) have higher values (closer to 1). The EJD is based on the assumption that annular points correspond to the locations where the leaflets (thin tissue) attach to the thicker tissue, and adds robustness to the detection, since WNCC only is sensitive to noise and cumulative errors.

A cost function is then defined as the linear combination of WNCC and EJD images:

$$C_i(x,y) = (1/2)W_i(x,y) + (1/2)E_i(x,y) \qquad (1)$$

where $W_i(x,y)$ and $E_i(x,y)$ are the WNCC and EJD images at cut-plane *i* and $C_i(x,y)$ is the corresponding cost image. The local maximum of $C_i(x,y)$ is used to update the locations of ROI and ROS images on each iteration.

Finally, the Dijkstra minimum cost path algorithm[5] is used to find the annular locations between consecutive pairs of user-defined points. To do so, a 3D directed weighted graph is constructed using each cost image $C_i(x,y)$ as the weight of graph's edges; a path that passes through regions that will most likely contain MA points is then defined, and the computed annular locations are then converted to 3D coordinates thus obtaining the 3D MA. This approach is more robust than the simple use of global maximum of cost images, since it ensures spatial smoothness and continuity between detected points in adjacent cut-planes.

2.4. Mitral leaflet segmentation

ML segmentation is fully automated and relies on the previously computed stack of 36 cut-planes and relevant detected MA points. Leaflets are constructed on each plane by computing a Dijkstra's minimum cost path between the corresponding pair of detected annular points, using gray-level intensities of the image as the weight of 2D graph's edges. This results into the leaflets medial axis on each of the 36 rotational cut-planes (Figure 2, top), whose points belonging are converted into 3D spatial coordinates to obtain a points cloud representing the leaflets surface.

2.5. Quantification of 3D parameters

Both 3D MA and ML point clouds were used to quantify the following parameters: the annular perimeter, as well as annular height, A-P and Al-Pm diameters, were obtained from a fourth order Fourier approximation of the 3D MA points cloud. A 3D polygonal mesh representing the annular surface was obtained by Delaunay triangulation, from which MA 3D surface area and 2D projected area were computed. Using the same approach, a 3D polygonal mesh was computed from the ML points cloud (Figure 2, bottom), from which ML 3D surface area was obtained, as well as the tenting volume, defined as the volume of the enclosed surface between the MA and ML surfaces, and maximum and mean tenting heights. Moreover, local ML thickness was computed by extracting the values of the distance transform through the previously obtained leaflets medial axis, resulting in:

$$t_{x,y} = 2d_{x,y}sp \qquad (2)$$

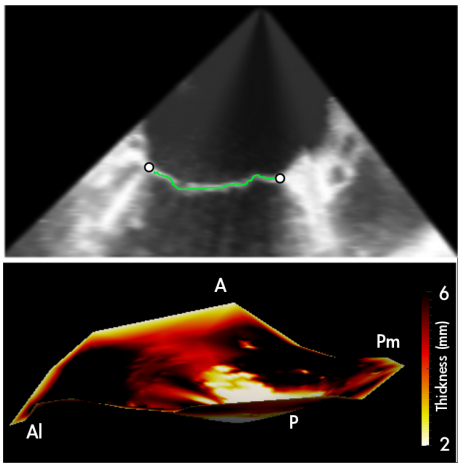

Figure 2. Leaflets segmentation and MV 3D polygonal mesh. Top: an example of a cut-plane with a pair of detected annular points (white circles) and the corresponding Dijkstra path delineating the leaflets (green stroke); bottom: resulting 3D mesh obtained using the annulus and leaflets points clouds, with regional leaflet thickness superimposed.

where $d_{(x,y)}$ is the value (in pixels) of the distance transform at (x, y) location and sp is the pixel spacing (in mm/pixel).

2.5.1. Reproducibility and validation protocol

To assess the reproducibility of the results with the proposed algorithm, two operators, blinded to each other, analyzed separately all the datasets. Moreover, to test for intra-observer variability, the first operator repeated the analysis twice. Both inter- and intra-observer variabilities were evaluated by the coefficient of variability (CV), defined as the absolute difference between the pair of measures in percent of their mean.

To test for the accuracy of the extracted parameters, the mean of the two measures obtained by the first operator was compared against a "gold standard", defined as the parameters (MA perimeter, A-P and Al-Pm diameters, height, 3D and 2D surfaces, ML exposed surface area) computed by a cardiologist using a conventional manual approach (MVQ-QLAB, Philips). Bland-Altman and linear correlation analyses were applied to determine the bias and limits of agreement as well as the coefficient of determination r^2.

3. Results

The initialization phase (VTK library-based) required $<$1 min, while the time required for MA and ML segmentation and quantification (in Matlab) was about 40 sec on a 2GB RAM, 2.26 GHz Intel Core Duo laptop.

Table 1 lists inter and intra-observer variability both for MA and ML parameters. The proposed algorithm showed a good level of reproducibility for most of these parameters. In particular, intra-observer reproducibility (CV$<$10%) was high for annulus perimeter, A-P and Al-Pm diameters as well as for surfaces and mean thickness. Conversely, height, tenting volumes and tenting heights were found as the least reproducible (CV around 20%).

In Table 2 the results of the comparison with the "gold standard" measures are reported. Optimal correlation, very small biases and narrow limits of agreement were found in all parameters except for the MA height, were the lowest accuracy, as shown by wide limits of agreement ($\pm$38.2%) and low r^2 value (0.556) was achieved.

4. Discussion

As the current main limit in widespread application of quantitative analysis of the MV apparatus from T3DE data is the time required for such analysis (about 10 minutes), our aim was to propose and test a nearly-automated method for MA and ML detection.

The implemented MA initialization step required only a limited number of points, and represented the only manual interaction during the whole segmentation. To ensure an adequate detection of the MA in the anterior part, in correspondence of the aortic valve, a denser initialization in that specific region was required, since intervalvular septum and leaflets exhibited similar thickness, thus potentially generating errors in detection. Moreover, the same approach could also be easily extended to segment the MA in open valves, since it relies on the thin-thick tissue interactions, intrinsic to the morphology of the MV. The ML segmentation was fully automated and, being not based on a geometrical or mechanical model but on the 3D information in the T3DE data, it allowed for the first time the computation of local leaflet thickness. Time required for this whole analysis was approximately one fifth of that needed by the manual conventional approach.

The validation results showed a very good agreement with the manual "gold standard" analysis, and good inter- and intra-operator reproducibility, except for the annular height and related tenting parameters. This is in agreement with Maffessanti et al[6], where repeatability of the manual measurements were investigated and the worst results obtained for MA height (inter: 17.2%; intra: 11.5%). Since MA height is defined as the maximum vertical distance between the saddle horn (the highest MA point) and the lowest MA point, it is expected to have an intrinsic variability as the saddle horn is located near the intervalvular (aorto-mitral) septum, which exhibits a similar thick-

Table 1. Inter and intra-observer variability results of MA and ML quantification. Values are presented as mean± standard deviation.

	Inter-observer variability			Intra-observer variability		
Parameter	Operator 1	Operator 2	CV (%)	Measure 1	Measure 2	CV (%)
MA perimeter (mm)	111.3±18.5	119.4±17.3	7.4±3.9	111.3±18.5	111.3±17.0	2.8±2.2
MA A-P diameter (mm)	30.1±5.4	33.6±6.5	9.6±6.2	30.1±5.4	29.3±5.6	4.7±3.3
MA Al-Pm diameter (mm)	36.7±5.6	39.3±6.0	8.0±4.9	36.7±5.6	36.5±5.8	3.7±3.4
MA height (mm)	5.7±2.3	6.4±2.7	26.3±14.7	5.7±2.3	5.7±2.0	21.7±12.3
MA 3D surface (cm^2)	9.4±3.0	10.4±3.4	13.1±8.2	9.4±3.0	9.2±3.0	8.7±7.1
MA 2D surface (cm^2)	8.8±2.8	9.7±3.2	12.8±7.2	8.8±2.8	8.7±2.8	7.4±6.6
ML 3D surface (cm^2)	13.4±3.9	15.1±4.1	12.3±7.9	13.4±3.9	13.6±3.8	6.6±4.4
ML mean thickness (mm)	2.6±0.8	2.7±0.9	6.6±3.3	2.6±0.8	2.6±0.8	3.8±3.0
Tenting volume (ml)	1.4±0.6	1.9±0.6	26.1±15.3	1.4±0.6	1.4±0.7	18.8±12.2
Tenting height (mm)	5.3±2.2	5.9±1.6	26.5±14.1	5.3±2.2	5.1±2.1	19.3±11.9
Mean tenting height	1.8±1.2	2.2±0.9	20.9±13.3	1.8±1.2	1.6±1.4	16.8±9.3

Table 2. Bland-Altman and linear regression results of MA and ML quantification. LA: limits of agreement for Bland-Altman analysis; m and b: linear regression coefficients; r^2: coefficient of determination. Values between parenthesis represent the percentage of the mean. Bias was computed as the difference between the measured value and the gold standard.

	Bland-Altman analysis		Linear regression		
Parameter	Bias	CI	m	b	r^2
MA perimeter (mm)	-1.4 (1.3%)	±8.0 (±7.2%)	0.994	-0.7	0.945
MA A-P diameter (mm)	2.2 (7.6%)	±4.0 (±14.0%)	0.894	5.073	0.869
MA Al-Pm diameter (mm)	-0.02 (0.07%)	±4.4 (±11.9%)	0.851	5.445	0.871
MA height (mm)	-0.2 (3.3%)	±2.2 (±38.2%)	0.937	0.181	0.556
MA 3D surface (cm^2)	0.2 (2.0%)	±1.7 (±18.1%)	0.943	0.701	0.919
MA 2D surface (cm^2)	-0.13 (1.4%)	±1.6 (±17.9%)	0.913	0.643	0.925
ML 3D surface (cm^2)	2.8 (13.2%)	±1.7 (±14.0%)	1.067	2.096	0.953

ness when compared with the anterior mitral leaflet, thus affecting its location in the initialization phase, due to the operator subjectivity and experience.

4.1. Limitations

Validation needs to be extended to a wide number of cases, including several MV pathologies. Moreover, the current implementation of the ML algorithm is not fully sensitive to prolapse, thus requiring further manual interaction for estimation of prolapsing volume.

5. Conclusion

We presented a fast model-free, nearly-automated algorithm for MA and ML segmentation and morphologic quantification from T3DE datasets. Validation against manual "gold standard" showed optimal agreement and very good reproducibility of the analysis, thus potentially representing a new tool for the MV evaluation in the clinical settings.

References

[1] Maffessanti F, Marsan N, Tamborini G, Sugeng L, Caiani E, Gripari P, Alamanni F, Jeevanandam V, Lang R, Pepi M. Quantitative analysis of mitral valve apparatus in mitral valve prolapse before and after annuloplasty: A three-dimensional intraoperative transesophageal study. J Am So Echocardiography 2011;.

[2] Schneider R, Perrin D, Vasilyev N, Marx G, del Nido P, Howe R. Mitral annulus segmentation from 3d ultrasound using graph cuts. IEEE Tran Med Im 2010;29(9):1676–1687.

[3] Schneider R, Burke W, Marx G, del Nido P, Howe R. Modeling mitral valve leaflets from three-dimensional ultrasound. Fun Ima and Mod of the Heart 2011;215–222.

[4] Schneider R, Tenenholtz N, Perrin D, Marx G, del Nido P, Howe R. Patient-specific mitral leaflet segmentation from 4d ultrasound. MICCAI 2011 2011;520–527.

[5] Dijkstra E. A note on two problems in connexion with graphs. N mathematik 1959;1(1):269–271.

[6] Maffessanti F, Stevanella M, Votta E, Lombardi M, Parodi O, de Marchi D, Conti C, Redaelli A, Caiani E. Feasibility of a novel approach for 3d mitral valve quantification from magnetic resonance images. In Computers in Cardiology 2010. IEEE, 2010; 157–160.

Address for correspondence:

Miguel Sotaquira
Department of Biomedical Engineering, Politecnico di Milano, Piazza L. da Vinci 32, 20133 Milano, Italy
miguel.sotaquira@mail.polimi.it